The Astrophysical Journal, 711:631–640, 2010 March 10 doi:10.1088/0004-637X/711/2/631

A METHOD FOR SEPARATING CORONAL MASS EJECTIONS FROM THE QUIESCENT CORONA

Huw Morgan and Shadia Habbal
Institute for Astronomy, University of Hawaii, 2680 Woodlawn Drive, Honolulu, HI 96822, USA; hmorgan@ifa.hawaii.edu
Received 2009 September 3; accepted 2010 January 21; published 2010 February 16

ABSTRACT

A method for separating coronal mass ejections (CMEs) from the quiescent corona in white-light coronagraph images is presented. Such a separation allows the study of CME structure, as well as enabling a study of the quiescent coronal structure, without contamination by the CME. The fact that the large-scale quiescent corona is very close to radial, whilst CMEs are highly non-radial, enables the separation of the two components. The method is applied to Large Angle Spectrometric Coronagraph/*Solar and Heliospheric Observatory* C2 and C3 observations, and is successful in revealing CME signal, faint CMEs and blobs, and dark rarefactions within a CME. The success of the separation is tested at solar minimum, a time when streamers are in general most non-radial. The technique is also compared to other commonly used methods. The separation method enables (1) the study of extremely faint CME structure, down to almost the noise level of the coronagraphs, (2) paves the way for automated categorization of CME internal structure, and (3) provides a cleaner basis for tomography of the quiescent corona, without contamination from CMEs.

Key words: solar wind – Sun: corona

1. INTRODUCTION

The slow realization that an outflow of material from the Sun could permeate the heliosphere and interact with the planets was made during, and following, the second half of the 19th century, before the modern model of the solar wind was finally established by Parker (1958). The first coronal mass ejection (CME) to be observed scientifically was during the total eclipse of 1860, but it was not recognized as the important dynamic phenomenon that they are (see review by Clark 2007). It was the white-light coronagraphic observations made by the Skylab mission in the early 1970s that led to the discovery of CMEs and the frequency of their occurrence; see Gosling et al. (1974) and references within.

CMEs are energetic clouds of magnetic plasma ejected by the Sun into interplanetary space. They have a large range of sizes, masses, and velocities. They are associated with the eruption of filaments and/or solar flares.

The Large Angle Spectrometric Coronagraph (LASCO) on board the *Solar and Heliospheric Observatory* (*SOHO*, Brueckner et al. 1995) enabled a great advance in our understanding of the dynamic corona, and paved the way for the Sun Earth Connection Coronal and Heliospheric Investigation (Howard et al. 2002) coronagraphs on the Solar Terrestrial Relations Observatory (STEREO) spacecraft. In the last decade, CME events (and their spatial size, type and distribution, velocity and acceleration) have been detected and cataloged using manual (Yashiro et al. 2004) and automated (Robbrecht & Berghmans 2004; Olmedo et al. 2008) methods, enabling detailed statistical analysis and revealing correlation with other solar events (e.g., Gopalswamy et al. 2001 or Bewsher et al. 2008).

Enhancing the appearance of CMEs in coronagraph observations involves the application of modern image-processing methods. Time differencing (or running difference images) is the most popular method, being robust and simple. A time-difference image shows the simple temporal differential. More sophisticated methods reveal CME structure by edge enhancement, which is a form of spatial differencing (see Byrne et al. 2009 and references within), or by wavelet decomposition, which locally enhances certain spatial frequencies and suppresses others (Stenborg & Cobelli 2003).

This work introduces a technique to isolate the CME and the quiescent corona components in a white-light image, resulting in separate images of the CME, and the background corona without a CME. Section 2 describes the quiescent-CME separation technique. Section 3 shows the results of applying the technique to LASCO C2 and C3 data containing CMEs. Section 4 discusses the results and potential applications for the technique. Conclusions are given in Section 5.

2. METHOD

Figure 1(a) shows a LASCO C2 total brightness observation of the corona made on 2000 January 1, 12:54. The displayed field of view is 2.2–6 $R_\odot$. The image is taken from a level 0.5 fits file (no radiometric calibration has been applied). A long-term minimum background has been subtracted. The long-term minimum image is not an exact image of the unwanted F-corona and instrumental stray light, but does help to effectively reduce these unwanted effects. This approach of background subtraction is suitable for image processing, but less suitable for quantitative analysis. For quantitative analysis, the data should be calibrated and a more careful background subtraction must be applied (see Morgan & Habbal 2007b, or Hayes et al. 2001). No CME can be seen in this image since the contrast is dominated by the steep drop of brightness with height.

Figure 1(b) shows the image brightness values along two circular paths at constant distance from the Sun center—3.0 and 5.5 $R_\odot$. The time-normalized counts in the 3.0 $R_\odot$ profile range from ∼10 to 150, whilst the counts at 5.5 $R_\odot$ range from ∼0 to 15. In fact, the average brightness is ∼30 and 4 at 3.0 and 5.5 $R_\odot$, respectively, and the standard deviation drops similarly. When both profiles are plotted on appropriate scales, it is clear that the basic large-scale structure of the corona is very similar at both heights. Scaling the brightness enables effective comparison of structure at both heights. It is possible to apply a similar scaling throughout the image. Figure 1(c) shows the average $B_{\rm av}$ and standard deviation σ of brightness as a function of height r in the image. The normalized brightness ($\tilde{B}$) shown in the image of Figure 1(d) is obtained from the brightness B of Figure 1(a)

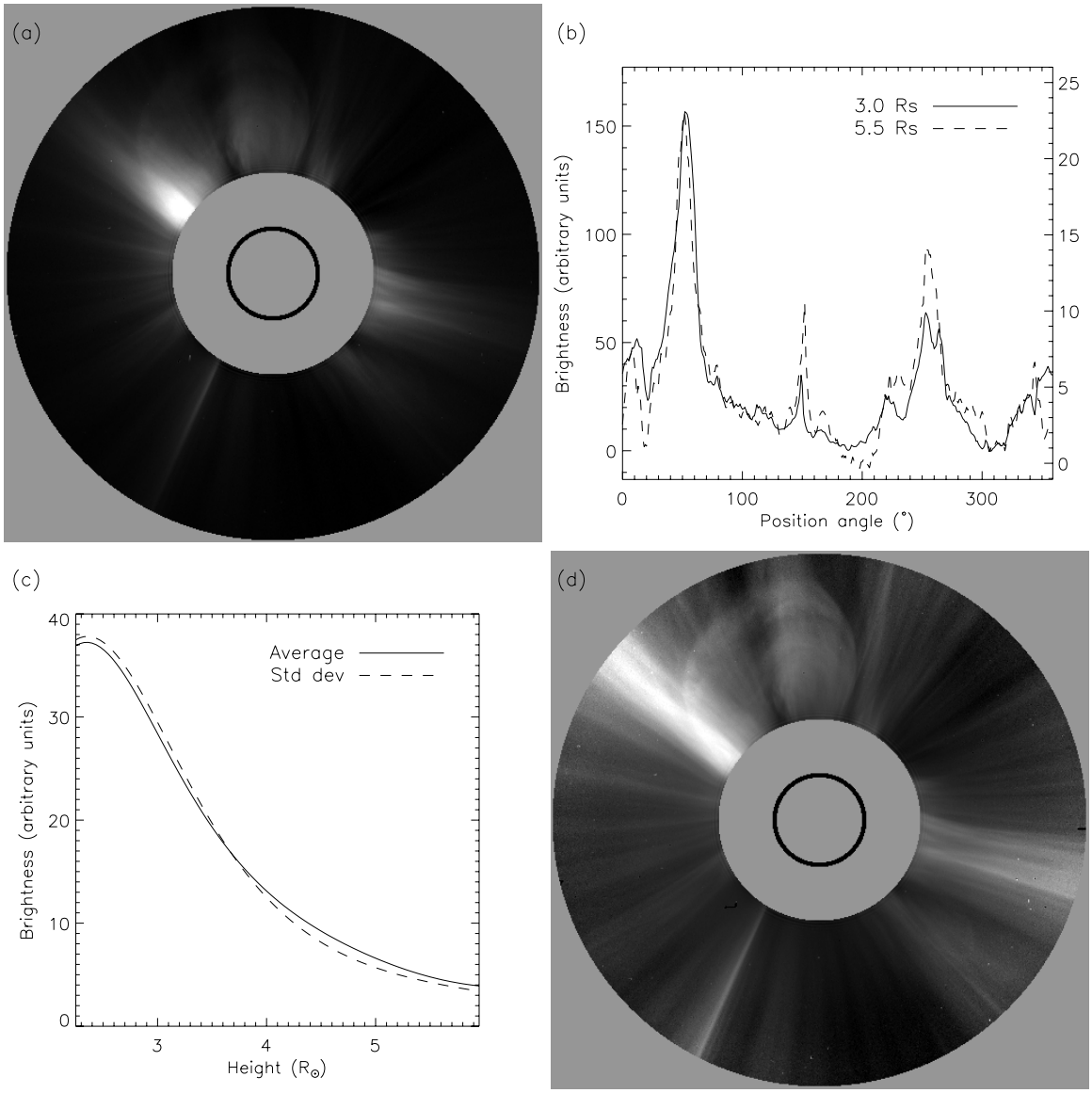

Figure 1. (a) Corona viewed from 2.2–6 $R_\odot$ by LASCO C2 on 2000 January 1 12:54 in total brightness. A long-term minimum image has been subtracted to reduce the effect of the F-corona and instrumental stray light. (b) Profiles of brightness as a function of position angle extracted from the LASCO image at two heights—3.0 and 5.5 $R_\odot$. The left *y*-axis relates to the 3.0 $R_\odot$ measurement, the right to 5.5 $R_\odot$. (c) The average and standard deviation of brightness as a function of height within the LASCO C2 image. (d) The image normalized using the average and standard deviation (NRGF processing—see text).

by

$$\tilde{B} = \frac{B - B_{\rm av}}{\sigma}. \quad (1)$$

Normalizing the image according to the average and standard deviation at each height is the basis of the Normalizing Radial Graded Filter (NRGF) described by Morgan et al. (2006). Figure 1(d) reveals the presence of a relatively faint CME in the north corona. It also reveals how close to radial the large-scale coronal structure is at heights above $\sim$3 $R_\odot$. This fact is often hidden by inaccurate image processing of coronagraph images. The only structure that is not radial is the CME, and this is the basis for the CME-quiescent corona separation method.

Before NRGF processing, iterative median noise reduction is applied to the image using the following method. A local median and standard deviation from the median is calculated throughout the image. Regions with large standard deviation are identified. If the area of the region totals 9 pixels or less, the pixels are replaced with the local median (determined over a region of 9 × 9 pixels). If the region is larger, the pixels are ignored in subsequent processing steps. In the examples shown in this article, there are no such large regions. The iterative median noise-reduction method is not necessary for simple image display, but is very robust for general analysis.

Figure 2(a) shows the NRGF-processed image of Figure 1(d) remapped into polar coordinates: position angle (measured counterclockwise from north) and height from Sun center *r*. Remapping into polar coordinates allows an easy calculation of the height-averaged brightness within the NRGF image (here, we mean the brightness of the NRGF image, or $\tilde{B}$, as given by Equation (1)). This can be calculated by summing over the columns, and dividing by the number of rows. This average is shown as the darker solid line in Figure 2(b). The shaded region surrounding the line shows ±1 standard deviation from the average. The small range of the shaded region reinforces what the eye can clearly see in the NRGF images—the coronal

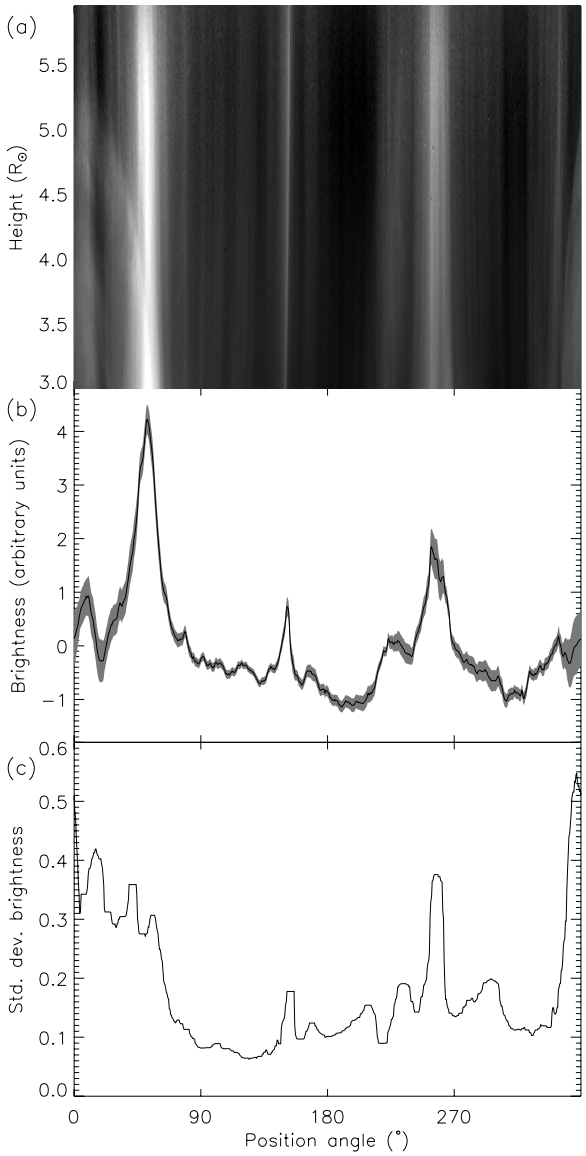

Figure 2. (a) LASCO C2 NRGF-processed image of Figure 1 remapped in polar coordinates. The *x*-axis shows position angle measured counterclockwise from north. (b) The height-averaged normalized brightness as a function of position angle. The shaded region shows $\pm\sigma$ (standard deviation) from the average. (c) σ as a function of position angle. To remove isolated outlying pixels, σ has been smoothed with a sliding median window 3° wide.

structure is very similar at all heights. Figure 2(c) shows more details of how the standard deviation varies across position angles. The standard deviation correlates in general with the average brightness, but increases at the position of the CME surrounding position angle 0°. This is to be expected—the CME introduces a variation in brightness which is not radial. Note that the final method used to isolate the CME signal from the quiescent corona depends on the quiescent corona having only a small slow variation in the radial direction. For this reason, the analysis has been limited to heights above 3 $R_\odot$, or where the quiescent corona becomes close to radial.

If the height-averaged brightness shown in Figure 2(b) is subtracted from each row of Figure 2(a), Figure 3(a) is obtained. Although this subtraction has enhanced the CME signal, it is not a valid process for isolating the CME for two reasons. (1) The brightness of the CME itself has been included in calculating the average, so that the average is too high in the regions containing a CME. (2) The large-scale structure of the corona is not purely radial. If fainter CMEs are to be revealed cleanly, a more sophisticated method for separating CMEs and the quiescent background corona is needed.

Figure 3(b) shows the result of a somewhat more sophisticated method. A height-smoothed image is obtained by running a sliding window or box-car average over the columns of the polar image of Figure 2(a), with a window width of ∼0.5 $R_\odot$. Note that no smoothing is applied in the position angle direction. Subtracting this height-smoothed image from the non-smoothed image isolates the higher frequency components in the height direction. This overcomes the problem of having a large-scale structure which is not purely radial. Any slow variation in NRGF brightness with height along a given position angle bin is removed by the high-bandpass filtering. This reveals very cleanly the CME near-position angle 0°. It also reveals a very faint CME near 230° (this faint structure is confirmed as a CME by applying the technique to several consecutive observations). However, the brighter CME structure is surrounded by dark bands due to subtracting the sliding window average. The CME and background are not truly separated in this case.

A more effective method is a two-step process. First, bright CMEs are detected using time differencing. Then regions containing CMEs are excluded from a calculation of the background average brightness. Figure 4(a) shows the image of Figure 2(a) with the previous observation (made approximately 20 minutes previously and identically processed), subtracted. Both observations are processed using the NRGF before the subtraction is made. This is an effective way of applying time differencing for CME detection. The quiescent coronal structure has changed little in the course of ∼20 minutes, so the subtraction removes this slowly changing component. The main CME is clearly revealed. The very small and faint CME is also revealed, but less clearly than in Figure 3(b). Dark bands lie within the bright structures of the main CME. These are at the position of the CME in the previous observation. This is one of the problems in interpreting time-differenced images. They are very effective in revealing dynamic events, but they should be used with care when analyzing the actual appearance, or structure, of the event.

Pixels in the time-difference image of Figure 4(a) with brightness values larger than a threshold of 3σ from the average (the average is more or less zero, as expected), are identified. A binary image of Figure 4(a) is produced, with the identified pixels set at 1 and the rest at 0. This image contains a lot of isolated pixel noise. Most of these are removed by a standard dilate-erode process, with a kernel, or submask of 3 × 3 pixels. The resulting binary image is shown in Figure 4(b). The black pixels show regions larger than 3 × 3 pixels where a significant change has occurred since the previous observation. These pixels will be excluded from calculating the background average brightness using the original image of Figure 2(a).

To calculate a background image for subtraction, each column of Figure 2(a) is processed separately. Figure 5 shows one such "slice." Pixels identified as belonging to a CME are ignored. The other pixels are fitted to a second degree polynomial. This fit is shown in Figure 5 as the solid line. When the fitted line (the background) is subtracted, the CME is left as a residue. This is repeated for all columns of Figure 2(a). The residual CME image can be cleaned by a 3 × 3 pixel sliding median window, which helps reduce spikes in isolated pixels without blurring larger features.

So far, the method has been applied to images in polar coordinates, which makes the image processing very simple. Once

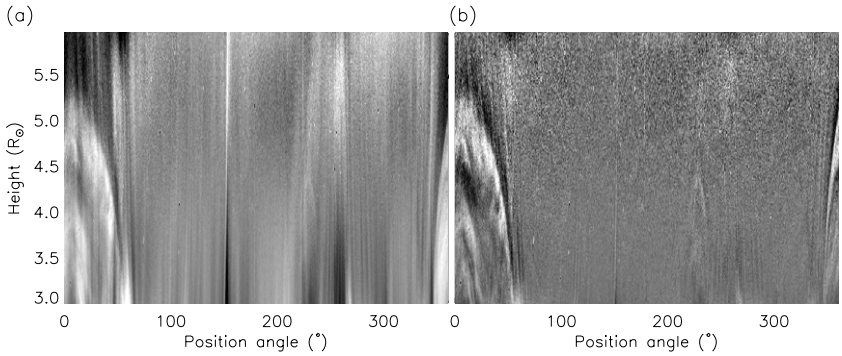

Figure 3. (a) Top image of Figure 2 with the height-averaged brightness subtracted. (b) Top image of Figure 2 with a sliding window average along the height direction subtracted.

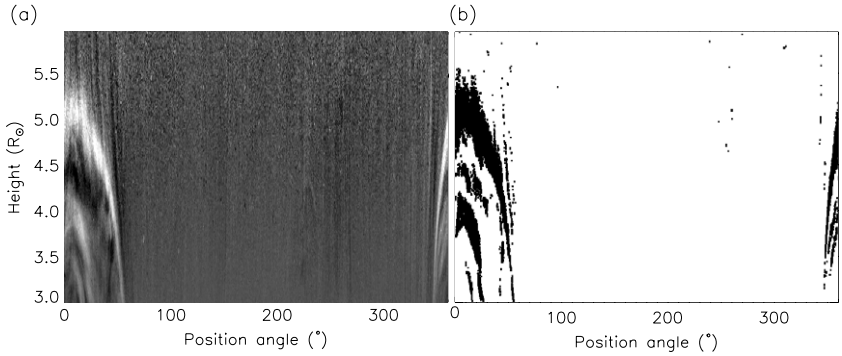

Figure 4. (a) Image of Figure 2(a) with the previous LASCO C2 observation, identically processed, subtracted. (b) Binary image where pixels in the left image with values larger than a threshold of 3σ from the average are shown black. To lessen noise detection of isolated pixels, a dilate-erode process has been applied after thresholding (see text).

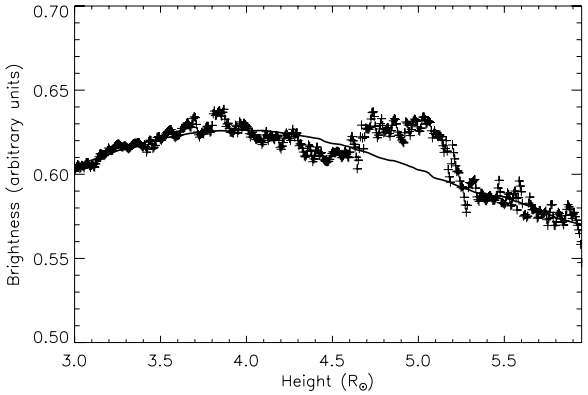

Figure 5. Crosses show brightness along one slice, chosen at position angle 10°, of the top image of Figure 2. The bright CME front edge is clearly seen at around 5 $R_\odot$. The solid line shows a polynomial fit to the brightness. The bright CME front edge has not been included in the polynomial fitting process.

the smooth background has been found using the polynomial fitting described in the previous paragraph, it is easy to map the background back into the cartesian coordinates of the original image. This remapped background can then be subtracted to reveal CMEs in the original image.

3. RESULTS

Figure 6 shows three examples of applying the technique to LASCO C2 and C3 data for the same day at roughly 3 hr intervals. The top row shows the observation discussed in the previous section, 2000 January 1, 12:54. In the CME component image on the right side of the row, the main CME is clearly revealed as a structure with a wide, bright front with footpoints extending down toward the Sun. Under the main front, smaller loops can be seen. A dark region is tucked behind the largest wide front. This is a real feature of the CME and not an artifact of the technique (this fact can be seen clearly in Figure 5, where a small dip follows the bright CME front). The extremely faint CME in the southwest is also revealed. Only a sequence of images taken over time identifies this faint feature as a small CME.

The middle row of Figure 6 shows another C2 image of 2000 January 1 taken later at 16:06. The main body of the north CME has passed beyond the C2 field of view, but trailing strands and dark voids can be seen in its wake. It is difficult to discern what is disturbed quiescent corona, and what is actually part of the propagating CME. In the southwest, a bright CME front is freshly erupted at exactly the same position angle as the extremely faint structure seen a few hours earlier.

The bottom row shows a LASCO C3 image of 2000 January 1 observed at 19:42. Both CMEs are seen in this image, and both seem to have suffered considerable structural deformation as they propagated from the inner corona to the heliosphere. The C3 CME image suffers badly from noise above ~18 $R_\odot$.

4. DISCUSSION

4.1. Effectiveness of the Method

In all three rows of Figure 6, the middle column shows the background corona component. In still images, the eye sees little evidence of CMEs left in these images. The clarity and strength of the CMEs seen in the right column (separated CME component), and the cleanliness of the quiescent corona in the middle column demonstrates the effectiveness of the method. However, in movies, the eye can see small changes in regions

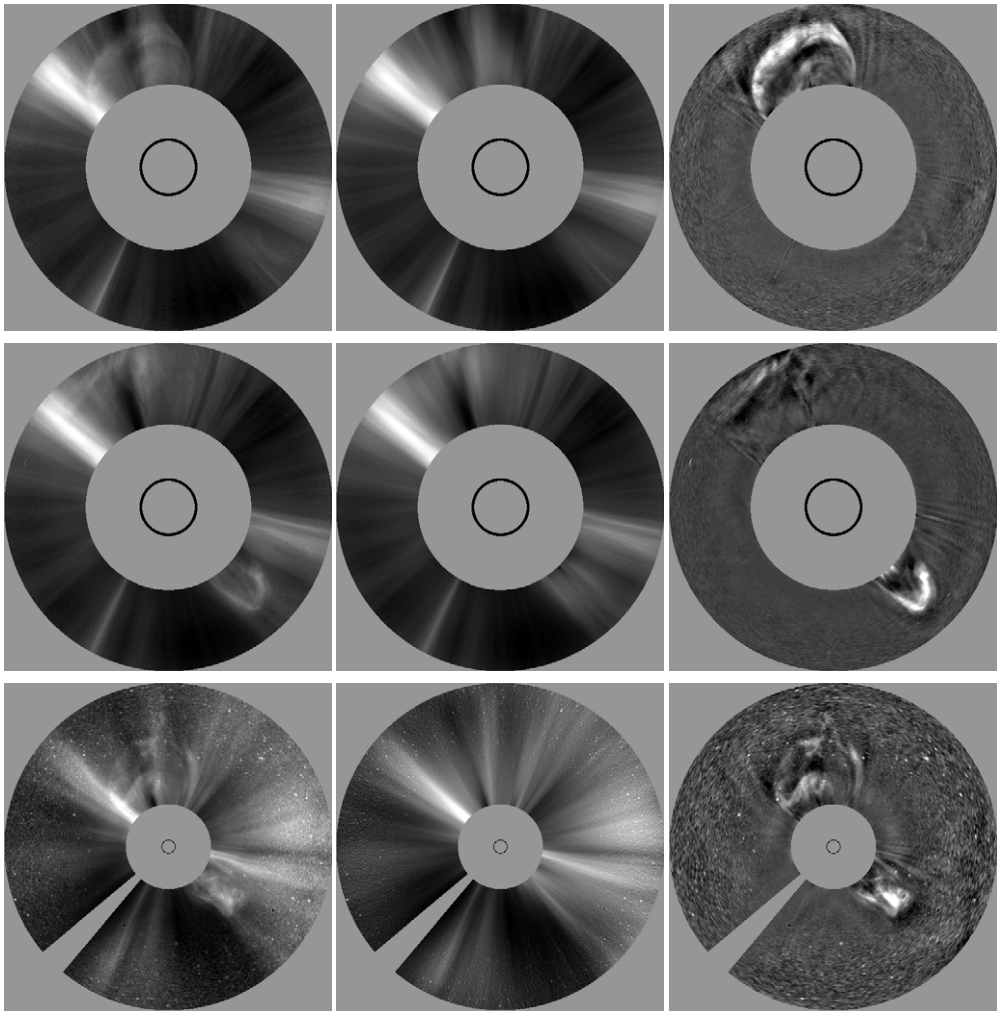

Figure 6. Top row: LASCO C2 observation of 2000 January 1, 12:54 (shown field of view is 3–5.95 $R_{\odot}$). Middle row: LASCO C2 observation of 2000 January 1 16:06. Bottom row - LASCO C3 observation of 2000 January 1, 19:42 (shown field of view is 5.95–25 $R_{\odot}$). Left column shows the NRGF-processed image. Middle column shows the background quiescent corona, and the right column shows the CMEs and other features, obtained by subtracting the middle column images from the left column images, and applying a 3 × 3 pixel sliding median filter.

that originally contained CMEs. This is to be expected, as the quiescent corona must be affected by the passage of CMEs. Additionally, it is likely that we have not achieved a perfect separation of the background quiescent corona and dynamic events.

4.1.1. Non-radial Quiescent Structure

The success of the separation is best tested at a time when coronal structures are as far from radial as possible. This puts the most demanding challenge on the separation method. For this purpose, we turn to data collected during 1997 February, a time close to solar minimum when streamers are restricted to low latitudes, and tend to deviate from radial toward the equator. Figure 7 shows observations by LASCO C2 from 1997 February 23. Figure 7(a) contains a CME, at 03:55, and Figure 7(b) is taken after the CME has passed, at 07:43. Profiles of normalized brightness as a function of position angle for the two observations are shown in Figures 7(c) and (d). The original normalized brightness, and the quiescent and dynamic separated components are shown. The quiescent corona is in most places indistinguishable from the original unseparated corona. The largest difference is seen, as expected, at the position of the CME. The dynamic component is very close to zero, barring small variations due to noise, at positions over the poles not containing streamers or CMEs. Near the equator, where streamers lie, there is a streamer structure which has contaminated the dynamic component of the image. This is at a significantly lower level than the CME signal seen near the east equator, and far lower than the quiescent corona signal. The separation is therefore good but not perfect. It should also be noted that there is considerable small-scale dynamic activity along the streamer belts, particularly in the west, with many small and faint blobs propagating along the current sheet. This contributes to the apparent "leakage" of quiescent structure signal in the dynamic component image. Figures 7(e) and (f) show the dynamic component images for the two observations, confirming what is already shown in Figures 7(c) and (d). The CME is by far the most dominant structure in the dynamic component, with some undesirable leakage from quiescent structure. During solar maximum, this leakage is less since the quiescent streamer structure is more radial.

4.1.2. Rapid Changes in Quiescent Structure

Streamers are often affected by the passage of a CME. Their mass content can change, resulting in a rapid change in brightness, and their spatial configuration can also change

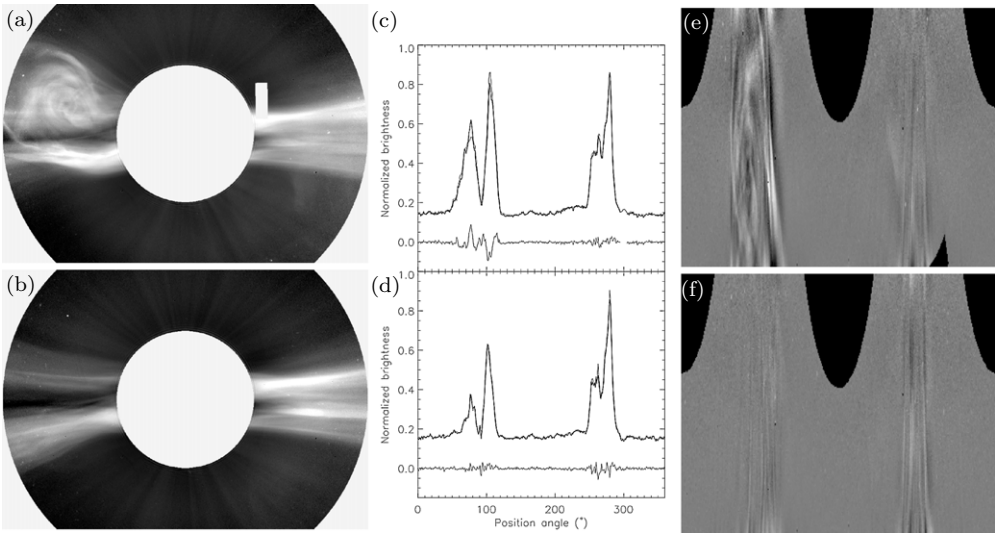

Figure 7. (a) NRGF-processed (no CME separation) image of a LASCO C2 observation made on 1997 February 23, 03:55. The shown field of view is 2.2–6 $R_\odot$ at the equator. A CME is blowing out the streamer just north of the east equator. (b) The same for 1997 February 23, 07:43, after the passage of the CME. The streamers have quickly settled to a close-to quiescent state. Note the drop in brightness of the north-east streamer. (c) A profile of normalized brightness as a function of position angle through the image of (a) at a height of 3 $R_\odot$ (bold solid line). Separation of the image yields the quiescent corona (lighter solid line almost hidden by the bold solid line), and the dynamic component (lighter solid line at values around zero). (d) The same as (c), but for the image of (b), which does not contain a CME. (e) The dynamic component image of (a), mapped in polar coordinates. (f) The same, but for the non-CME image of (b).

rapidly. This means that the quiescent coronal streamers, which we are attempting to separate from the dynamic CMEs, are themselves dynamic. The criterion for separation is a high-frequency deviation from a smooth curve in height-normalized brightness along a radial direction. This does not prevent, therefore, the quiescent component from containing temporal changes through a series of observations. In fact, we should expect the quiescent component to include temporal changes. However, care must be taken since components that should belong to the CME could contribute to the quiescent component.

A good example is shown in Figure 8. Looking at the south corona during 2002 August 6–7, LASCO C2 observes a bright and fast-moving CME. Figure 8(a) is a position angle–time plot of the event for the separated dynamic component. Figure 8(b) shows the same for the quiescent component. As shown in Figure 8(a), this CME passes through a height of 3 $R_\odot$ close to 18:00 on 2002 August 6. It is a very rapid event, as seen in Figure 8(a). A streamer associated with the CME is seriously disrupted for several hours. The streamer seems to suddenly split in two, before gradually joining again over the course of approximately 10 hr. The quiescent corona does not contain the structure of the CME, but does contain its rapid temporal effect on the streamer. This is more clearly shown by the series of images of the south corona over this time period in Figure 8(c). The three rows of images are NRGF processed, with no separation, in the top row, the dynamic separated component (middle row) and the quiescent component (bottom row). In the absence of a CME, the dynamic component is very clean—almost no quiescent streamer structure has contaminated these images, which is typical when applying the method to the radial solar maximum corona. The quiescent coronal images show the brightest streamer splitting in two as the CME passes, then gradually joining back together at all heights by the last image. These images show the quiescent corona changing quite rapidly hours after the main CME event has passed. This suggests that the temporal changes in the quiescent coronal images revealed by the separation method are a reliable indication of true changes in the streamer structure, and are not errors caused by CME signal "leaking" into the quiescent component. However, as stated earlier, there may well be some small CME contribution to the quiescent component, just as there is some small quiescent contribution to the dynamic component. This is unavoidable without a more sophisticated separation method, and may well be impossible without improved observations.

4.1.3. Histogram Analysis

Figure 9 demonstrates the effectiveness of the separation method by histogram analysis. Figures 9(a) and (b) are based on a LASCO C2 observation made during 2000 January 1 in the absence of CMEs. The solid line in Figure 9(a) shows the histogram of NRGF brightness (without any quiescent–dynamic separation) in a polar coordinate image. This distribution is typical of the NRGF-processed corona, with a negative most probable brightness (or peak). Recall the average brightness in an NRGF image is zero. The distribution is skewed, with a gradual decrease from the peak to high brightness. The distribution is generally smooth, and generally a larger variation from a smooth distribution is seen at higher brightnesses. The dashed line shows the quiescent corona, obtained by the separation method. The quiescent corona is very similar to the total corona. Figure 9(b) reveals the separated dynamic corona as a narrow symmetrical distribution centered on zero, and with an FWHM of approximately 0.15—far narrower than the range of brightnesses seen in the original image. The separated dynamic corona in this case must be mostly noise. The background quiescent corona is formed by a second degree polynomial fit to the non-dynamic corona, and so contains virtually no noise. The residual CME image contains all the noise, as well as the interesting dynamic features. Figures 9(c) and (d) show the same as Figures 9(a) and (b) respectively, but for the image of 2000 January 1, 12:54 shown previously in Figure 2(a). The main difference between Figures 9(d) and (b) is the presence of the CME in Figure 9(d), which shows as an extended wing at higher brightnesses. The number of pixels with this higher brightness is small (note the y-axis is base 10 logarithmic), but they are clearly separated from the background noise.

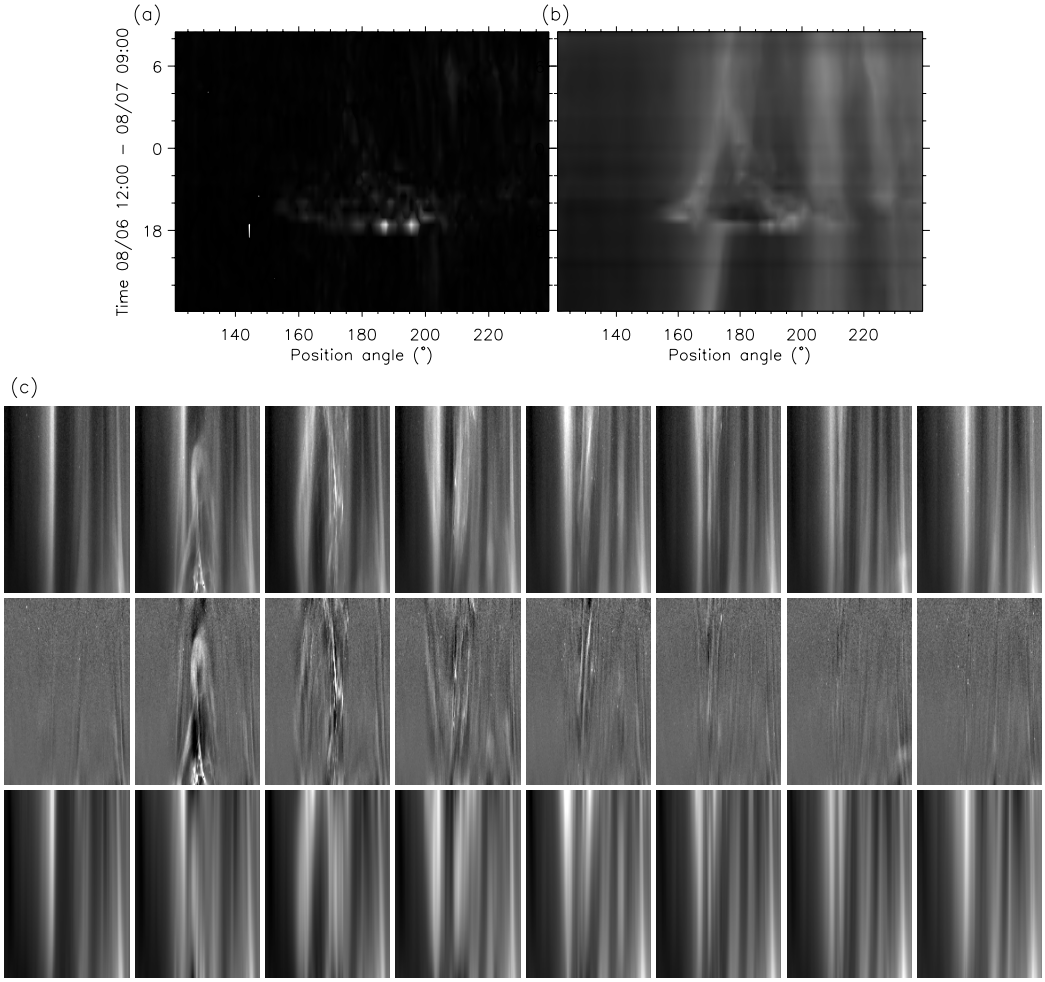

Figure 8. Position angle–time plots of brightness at a height of 3 $R_\odot$ for (a) the dynamic and (b) the quiescent separated components of LASCO C2 data collected between 2002 August 6 and 2002 August 7. Profiles of brightness at constant height are collected between position angles 120 and 240°, and stacked in time to create these plots. (c) Series of LASCO C2 observations covering the passage of the CME shown in part (a). Each image is in polar coordinates, with the displayed section of the corona between 2.5 and 6 $R_\odot$ (increasing vertically), and position angles between 120 and 260° (left to right). The time series of eight observations goes from left to right. The images in the top row are NRGF processed. The middle row is the separated dynamic component. The bottom row shows the separated quiescent component.

4.2. Comparison with Other Techniques

The technique outlined in this paper is more than simply an image-processing technique; it is an attempt to separate the dynamic and quiescent components, enabling further and more involved analysis of the CME and quiescent corona. However, it may be used as an image-processing method to view CMEs. In this section, we briefly compare the technique with other commonly used image processing approaches. A very complicated and filamentary CME structure propagates through the south corona during 2002 August 6, and is observed by LASCO C2. The observation is processed in different ways, and the results are shown in Figure 10. The following is a qualitative discussion of the results.

1. Figure 10(a) is a NRGF image of the whole corona. The process is effective at showing the quiescent corona and CME simultaneously.
2. Figure 10(b) uses the standard LASCO image processing, based on taking the ratio of the observation to a long-term minimum image, and applying heavy contrast enhancement. Such a method is robust but is not useful for comparing coronal structure or CMEs at all heights within the

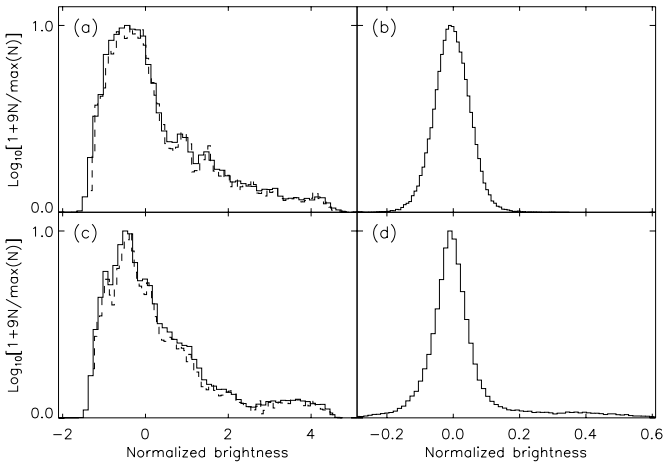

Figure 9. Histogram of brightness in processed images: (a) NRGF LASCO C2 image in the absence of CMEs taken earlier during 2000 January 1 (solid line) and of the background quiescent corona, separated from dynamic events (dashed line). (b) The dynamic component (mostly noise in this case). (c) As (a), but for the image including a CME of Figure 2(a). (d) The dynamic component of Figure 2(a). Notice the extended band of higher brightness, distinct from the noise. For clarity, the histogram values have been scaled between 1 and 10, and logged to base 10.

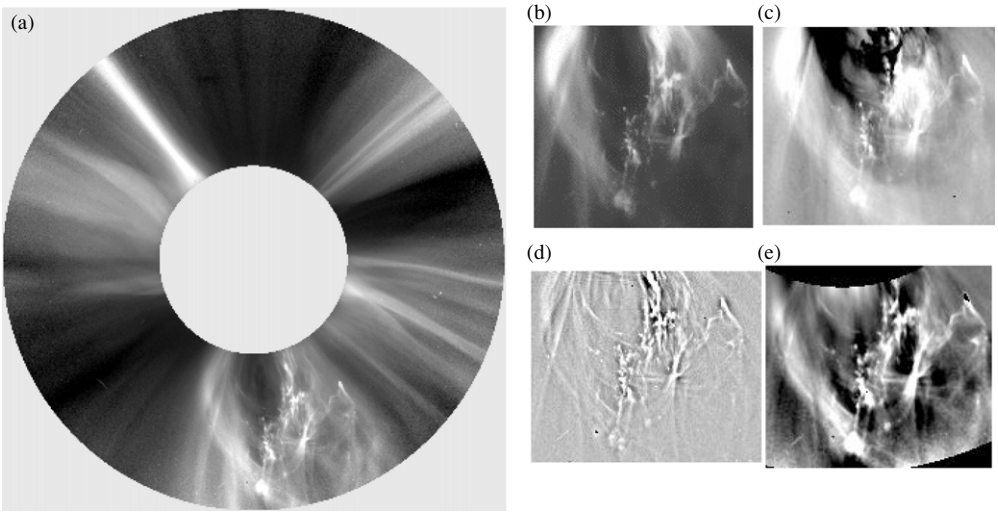

Figure 10. (a) NRGF-processed (no CME separation) image of a LASCO C2 observation made on 2002 August 6, 18:55. The shown field of view is 2.2–6 $R_{\odot}$. A bright and complicated CME is propagating through the south corona. Four close-up images of the CME in the south corona are shown processed from the original data using (b) the standard LASCO Solar Software image processing, (c) running difference, (d) wavelet decomposition, and (e) the CME separation method.

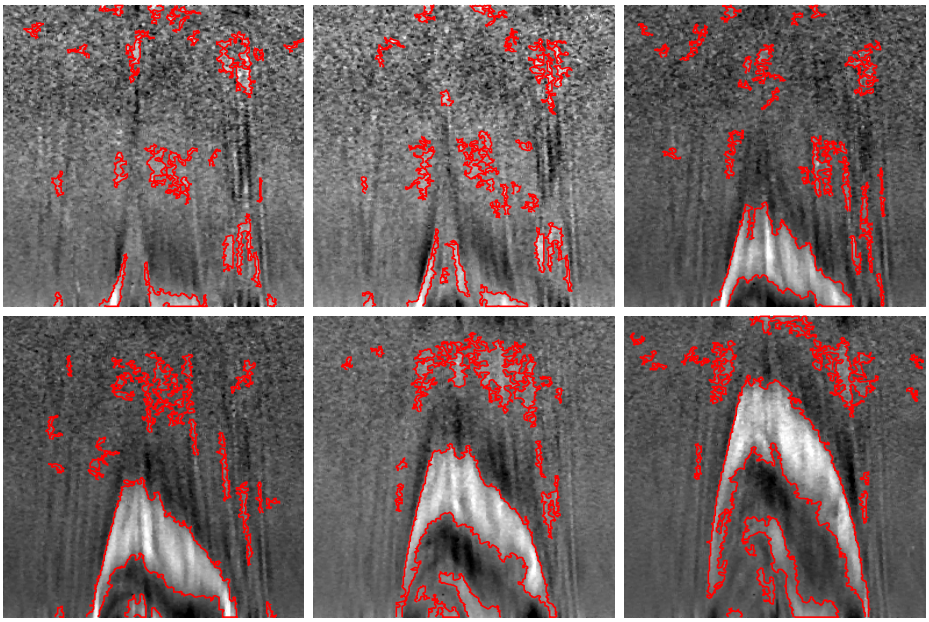

Figure 11. Region of interest analysis applied to the series of LASCO C2 observations. The images are in polar coordinates, showing the region between position angles −20° and 60°. Red contours outline the regions of interest (see text for more detail).

field of view. Details are lost by the contrast enhancement, and the structure is misleading.

3. Figure 10(c) is a running difference image. The CME structure is obscured by dark regions at the position of the CME in the previous observation. Another time-differencing method would be to take an observation of the corona prior to the CME, and subtract it from subsequent images. Problems then occur when streamers change brightness and position (due to the CME or due to slow changes in the quiescent corona and coronal rotation).
4. Figure 10(d) is a wavelet decomposition image, where higher spatial frequencies are enhanced. This image is a skeleton-type depiction of the corona structure, useful for revealing fine structural detail. However, the image is far removed from the true coronal structure, with brightness values unrelated to the true observed brightnesses.
5. Figure 10(e) shows the dynamic component after the CME separation technique. CME structure is revealed in detail at all heights, helped by the reduced background coronal brightness. The separation method yields the complicated structure filling the field of view, and the few narrow quiescent streamer structures seem to be entangled and drastically disturbed by the CME. In contrast to the other techniques, brightness values of the CME are preserved. Indeed, the original radiometrically calibrated brightness of the CME may be established using the separation technique, and a density calculated if one assumes a geometry to the CME (see Section 4.4).

4.3. Region of Interest Analysis

The separation method gives a unique tool to study CME structure, without the complexities of the interpretation of time-differenced images. In Figure 11, a series of images shows the

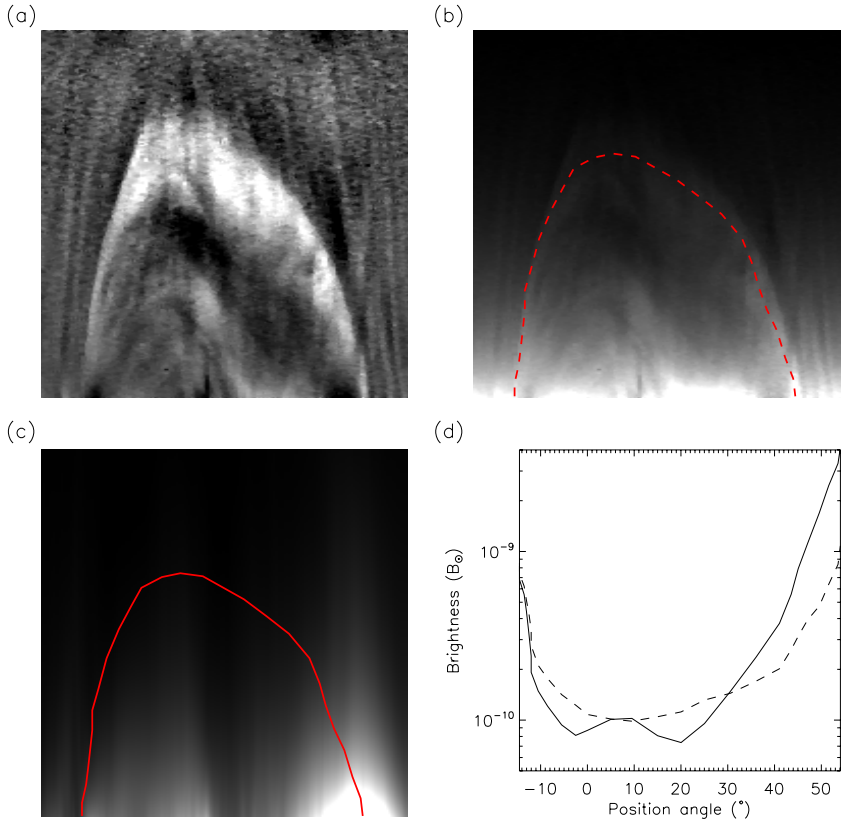

Figure 12. (a) LASCO C2 CME component shown in detail. (b) The same image transformed back to quantitative units, using the reverse of the NRGF process. The red dashed line traces the main front edge of the CME. (c) Same as (b), but for the background quiescent corona. The solid line follows the same path as the dashed line in (b). (d) Brightness values along the red lines in (b) and (c). The solid line shows brightness in the quiescent corona, and the dashed in the CME.

development or propagation of the CME through the C2 field of view. The red contours show regions of interest (ROI). The ROI have been identified as follows.

1. Pixels with values higher than one standard deviation of the main noise distribution shown in Figure 9(d) (0.08) are identified.
2. A binary image, initialized to zero, has all these identified pixels set to 1. These are candidate CME pixels.
3. A dilate-erode operator is applied. This removes isolated noisy pixels, and also groups closely spaced candidate pixels together.
4. Only regions containing more than 80 pixels are kept as candidate CME regions.
5. These regions are contoured on the images of Figure 11.

It is clear that the main structures of the CMEs are identified by the ROI method. Other clumps of closely spaced ROI seem to show only noise. However, they are localized, and the clumps seem to move consistently from one observation to the next. This is not typical behavior for noise. Therefore, a more sophisticated analysis is needed. A method which takes into account how ROI move from one frame to the next will distinguish between noise and true structure. It is interesting that the ROI analysis seems to detect a faint front edge to the CME, leading the bright main body. Such an ROI analysis, made possible by separating the quiescent and dynamic components, will lead to an automated procedure to catalog the internal structures of CMEs. It will also lead to new discoveries since it reveals faint structure not immediately obvious to the eye. This type of ROI analysis will be the subject of another publication.

4.4. Quantitative Analysis

One of the advantages of the NRGF process is that it is reversible. Having used the average and standard deviation of brightness as a function of height to flatten the image using Equation (1), the processed image can be converted back to the original brightness values by

$$B = \tilde{B}\sigma + B_{\rm av}. \quad (2)$$

This conversion can be applied to the separated background quiescent coronal image to regain the corona in calibrated rather than normalized units. Converting these components back to quantitative units by this method enables quantitative analysis of the CME or of the background. This is illustrated in Figure 12, where the brightness along the main bright edge of the CME is shown in mean solar brightness units, and compared to the background quiescent corona. In summary, the NRGF process flattens the image in a way that enables the separation of quiescent and dynamic corona. Then, the separated components can be transformed back to radiometric units of mean solar brightness. This is extremely useful for estimates of density in different parts of the CME. A note of caution here—the accuracy of the analysis depends directly on the accuracy of the radiometric calibration and the accuracy of the F-corona and instrumental stray light background subtraction (see Morgan & Habbal 2007b and references within for more discussion of background subtraction with radiometrically calibrated data).

5. CONCLUSIONS

A method for separating CMEs from the quiescent corona in white-light coronagraph images is presented. The NRGF

process flattens the dominant radial gradient in brightness from the images. This is the vital step that enables separation of the close-to-radial quiescent coronal structure and the CME at higher spatial frequencies. A time-differencing method reveals which pixels contain CME signal and the remaining pixelsn are used to fit a smoothly changing quiescent corona to a polynomial. Subtracting this quiescent corona isolates the CME signal.

The method results in a clean and effective separation of the large-scale quiescent corona and dynamic events. Isolating CMEs in observations from many viewpoints (such observations are now routine with the ongoing observations of LASCO combined with the STEREO coronagraphs) will allow well-constrained estimates of the true three-dimensional CME structure (see Frazin et al. 2009). The CME component image gives a direct representation of the CME structure. This is in contrast to, for example, time differencing. In a running-difference image, there are bright ridges where the CME lies in the most recent frame under consideration, and dark regions where the CME was in the previous frame. CMEs are complex structures, with multiple bright features following each other through the corona. Running difference images are not good images to interpret CME structure. An advantage of this method compared to time differencing, wavelet decomposition, or edge enhancement is that it reveals the direct observed brightness of the CME, in calibrated units. As well as gaining a direct, isolated measurement of a CME, one also gains measurements of the corona minus CMEs. This background corona is actually a polynomial fit to the observed corona (a polynomial fit along the radial direction—see Section 2), so is very smooth and clean. Sets of such clean, slowly varying images are useful for solar rotational tomography (SRT), or other inversion methods, to reveal the quiescent coronal structure or density. CMEs can seriously deteriorate the results of such inversion methods, as the inversion attempts to incorporate the CME in the coronal structure. A standard approach is to remove images which contain CMEs, but this is of course a problem at solar maximum since it leaves very few observations to work with. We will soon use the separated quiescent images with the SRT techniques of Morgan et al. (2009). However, the method works well only for regions of the corona which are radial, or very close to radial (approximately 3 to 25 $R_\odot$). Below 3 $R_\odot$, the coronal structure is far from radial. Coronal structures which are not necessarily associated with CMEs such as bright narrow non-radial rays (see Morgan & Habbal 2007a) will be contained in the final isolated CME image. In general, above $\sim$25 $R_\odot$, even a perfectly radial corona would not appear radial due to the Thomson sphere. In addition, for observations above 25 $R_\odot$, the biggest challenge lies in removing noise, stars/objects, and the F-corona brightness (see Lugaz et al. 2009), not in applying more sophisticated image processing.

The software for applying the separation technique will be made available to the community by incorporation into the Solar Software package soon. Separated dynamic and quiescent coronal images will be made available via the Institute for Astronomy, University of Hawaii Solar Images website (http://alshamess.ifa.hawaii.edu/).

This work was supported by NASA grant NNX08AJ07G to the Institute for Astronomy. Huw Morgan thanks Richard Frazin (University of Michigan) for previous discussions on separating CMEs from background corona. We thank the anonymous referee for suggestions which have greatly improved this article. The *SOHO*/LASCO data used here are produced by a consortium of the Naval Research Laboratory (USA), Max-Planck-Institut fuer Aeronomie (Germany), Laboratoire d'Astronomie (France), and the University of Birmingham (UK). *SOHO* is a project of international cooperation between ESA and NASA.

REFERENCES

Bewsher, D., Harrison, R. A., & Brown, D. S. 2008, A&A, 478, 897
Brueckner, G. E., et al. 1995, Sol. Phys., 162, 357
Byrne, J. P., Gallagher, P. T., McAteer, R. T. J., & Young, C. A. 2009, A&A, 495, 325
Clark, S. 2007, The Sun Kings (ESA-SP 446; Princeton, NJ: Princeton Univ. Press)
Frazin, R. A., Jacob, M., Manchester, W. B., Morgan, H., & Wakin, M. B. 2009, ApJ, 695, 636
Gopalswamy, N., Yashiro, S., Kaiser, M. L., Howard, R. A., & Bougeret, J.-L. 2001, J. Geophys. Res., 106, 29219
Gosling, J. T., Hildner, E., MacQueen, R. M., Munro, R. H., Poland, A. I., & Ross, C. L. 1974, J. Geophys. Res., 79, 4581
Hayes, A. P., Vourlidas, A., & Howard, R. A. 2001, ApJ, 548, 1081
Howard, R. A., Moses, J. D., Socker, D. G., Dere, K. P., & Cook, J. W. 2002, Advances in Space Research, 29, 2017
Lugaz, N., Vourlidas, A., Roussev, I. I., & Morgan, H. 2009, Sol. Phys., 256, 269
Morgan, H., & Habbal, S. R. 2007a, A&A, 465, L47
Morgan, H., & Habbal, S. R. 2007b, A&A, 471, L47
Morgan, H., Habbal, S. R., & Lugaz, N. 2009, ApJ, 690, 1119
Morgan, H., Habbal, S. R., & Woo, R. 2006, Sol. Phys., 236, 263
Olmedo, O., Zhang, J., Wechsler, H., Poland, A., & Borne, K. 2008, Sol. Phys., 248, 485
Parker, E. N. 1958, ApJ, 128, 664
Robbrecht, E., & Berghmans, D. 2004, A&A, 425, 1097
Stenborg, G., & Cobelli, P. J. 2003, A&A, 398, 1185
Yashiro, S., Gopalswamy, N., Michalek, G., St. Cyr, O. C., Plunkett, S. P., Rich, N. B., & Howard, R. A. 2004, J. Geophys. Res. (Space Phys.), 109, 7105